Performance Improvement of a High-Speed Swimming Robot for Fish-Like Leaping

Di Chen, *Graduate Student Member, IEEE*, Zhengxing Wu, *Member, IEEE*, Pengfei Zhang, Min Tan, and Junzhi Yu, *Fellow, IEEE*

***Abstract*—Many aquatic animals are able to leap out of water effortlessly, however, it is still exceedingly challenging for a swimming robot. Inspired by the fast-swimming mechanism of fish, in this letter, we develop an untethered high-speed swimming robot with the integration of high-frequency oscillation and compliant passive components for performance improvements in swimming speed, efficiency and even fish-like leaping motion. The stiffness optimization of compliant components is conducted via experiments. As a result, both swimming speed and efficiency have been significantly improved and the robot surprisingly reaches a swimming speed of 1.88 m/s corresponding to 7.1 body lengths per second (BL/s). That is, the compliant components' stiffness is of great importance to the performance improvement of a swimming robot at high-frequency oscillation. Additionally, the leaping motion is successfully performed with the optimized swimming robot and the maximum height of center of mass (CM) can reach up to 0.23 m. A simplified model is developed to analyze the leaping height with different speeds and body lengths, which suggests that the robot with small size leaps out of water more easily. The obtained results in this letter will offer some significant insights into the design and optimization for a high-speed swimming robot, as well as the cross-domain motions between water and air.**

***Index Terms*—Biologically-inspired robots, mechanism design, compliant joints and mechanisms, high-speed swimming, fish-like leaping motion.**

Manuscript received August 31, 2021; accepted December 30, 2021. Date of publication January 13, 2022; date of current version January 24, 2022. This letter was recommended for publication by Associate Editor J. Liu and Editor X. Liu upon evaluation of the reviewers' comments. This work was supported in part by the National Natural Science Foundation of China under Grants 62022090, 61973303, 61725305, U1909206, and T2121002, in part by the Beijing Natural Science Foundation under Grant 4192060, and in part by the Youth Innovation Promotion Association CAS under Grant 2019138. *(Corresponding author: Junzhi Yu.)*

Di Chen, Zhengxing Wu, Pengfei Zhang, and Min Tan are with the School of Artificial Intelligence, University of Chinese Academy of Sciences, Beijing 100049, China, and also with the State Key Laboratory of Management and Control for Complex Systems, Institute of Automation, Chinese Academy of Sciences, Beijing 100190, China (e-mail: chendi2018@ia.ac.cn; zhengxing.wu@ia.ac.cn; zhangpengfei2017@ia.ac.cn; min.tan@ia.ac.cn).

Junzhi Yu is with the State Key Laboratory for Turbulence and Complex Systems, Department of Advanced Manufacturing and Robotics, BIC-ESAT, College of Engineering, Peking University, Beijing 100871, China, and also with the State Key Laboratory of Management and Control for Complex Systems, Institute of Automation, Chinese Academy of Sciences, Beijing 100190, China (e-mail: junzhi.yu@ia.ac.cn).

This letter has supplementary downloadable material available at https://doi.org/10.1109/LRA.2022.3142409, provided by the authors.

Digital Object Identifier 10.1109/LRA.2022.3142409

I. Introduction

IN NATURE, a variety of aquatic animals own excellent swimming performance in speed, maneuverability, and efficiency, which offers numerous sources of inspiration for the design of swimming robots [1]. More impressively, many of them with a wide range of scale are also expert in leaping out of water for escaping from predators, capturing prey, migration, and even merely recreating. The mechanisms of swimming have been investigated for many years [2]. Strenuous efforts in the development of swimming robot have been made to chase after the performance of real fish, especially in terms of swimming speed [3]. With the leaping motion, swimming robots can adapt more complex environment, such as intertidal zone and swamp. Although many achievements [4], [5] have been obtained, the extraordinary leaping is still technically challenging for a swimming robot.

To date, a large number of robots with the capability of jumping from ground have been developed, and impressive performances have been achieved [6], [7]. However, in contrast to jumping on solid ground, transiting from water to air poses more substantial challenges. Zhao *et al.* designed a water strider-inspired jumping robot which can continuously jump on water surface with a height of 120 mm [8]. Jiang *et al.* used the carbon fiber strip as energy storage component to design a water surface jumping robot which can jump up to 95 mm [9]. Recently, some aerial-aquatic robots have been developed to transmit from water to air. For example, Wood *et al.* developed a 175-milligram robot with a pair of piezoelectric actuators [10]. It can realize the flap motion in both water and air, as well as impulsively take off from water surface by igniting the oxyhydrogen with a sparker. Kovač *et al.* employed high-power-density solid reactants as the power of jet propulsion to design an aerial-aquatic robot which can launch from water surface into air rapidly and achieve a flight distance of 26 m [11]. From mentioned above, these robots mainly focus on the interface transition from water to air and all belong to impulsive jumpers which are initially at rest near water surface and then escape water surface with impulsive propulsion. In this way, they all achieve excellent jumping performances. However, most of them are not proficient in the underwater locomotion. Moreover, many of them are insect-scaled and tethered robots with simple mechanism, which cannot meet the requirements of tasks in complex aquatic environments.

Actually, many swimming animals with the capability of excellent swimming motion and leaping motion, such as flying fish

and dolphin, are often regarded as momentum jumpers or mixed jumpers [12]. Namely, they need more or less distance to reach an enough speed to exit water. The jumping performance depends critically on the exiting speed. The archerfish accelerates from near water surface with the propulsion of caudal fin and can jump up to 2.5 BL in height [13]. More surprisingly, flying fish can reach water surface at a speed of 10 m/s and a final take-off speed of 20 m/s, and then glide for a long distance in air [14]. In the past decades, a large number of works have been conducted to improve the speed of swimming robots. iSplash-II achieves an impressive speed of 11.6 BL/s with a tail-beating frequency of 20 Hz [15]. Zhu *et al.* developed Tunabot with a speed of 4.0 BL/s at 15 Hz [16]. By increasing the body flexibility, Tunabot Flex improves its performance to 4.6 BL/s with a beating frequency of 8.0 Hz [17]. However, the tethered swimming and pool maneuvers impede the leaping motion severely. To the best of our knowledge, there are only two biomimetic swimming robots can realize the leaping motion. Yu *et al.* developed a robotic dolphin with a speed of 2.85 BL/s [18]. Relying on excellent posture control, the robot can leap out of water agilely. In our previous work [19], a robotic fish can achieve a speed of 3.8 BL/s and autonomous leaping motion. However, owing to the limitation of speed, their leaping heights are still less. Inspired form the compliant mechanism of fish, many researchers have proposed variable-stiffness structures for better performance [20]–[23]. Chen *et al.* developed a fish robot with serial variable-stiffness joints [21]. By changing the stiffness distribution during swimming, the performance can be enhanced tremendously. Zhong *et al.* designed a robotic fish with the integration of a high-frequency actuation system and tunable-stiffness joint, which ensures the high efficiency during the fast swimming [23]. Therefore, it will be helpful to obtain better performance by integrating the high-frequency oscillation with the optimization of stiffness.

For the purpose of performing excellent leaping motion on a swimming robot, in this letter, we mainly focus on the design and performance improvements of a fast-swimming robot. First, a second-generation robot with the improved design in actuation system and structure parameters is developed. Second, the effects of compliant components' stiffness on swimming performance involving speed and efficiency are analyzed via experiments. With the obtained results, the optimization of proposed compliant joint under high-frequency oscillation demonstrates remarkable improvements in swimming performance. Furthermore, based on the optimized swimming robot, we perform the experiments and numerical analyses of leaping motion to explore its capability in height. The results of our robot have demonstrated its great potential in adapting complex aquatic environment and evolving into an aquatic-aerial robot by equipping with a pair of foldable fins.

The remainder of this letter is organized as follows. In Section II, mechanical design and prototype of the swimming robot are presented. Section III describes the swimming performance optimization with experiments. The performance testing and numerical analysis of leaping motion are conducted in Section IV. Section V gives detailed discussions. Finally, conclusions are presented in Section VI.

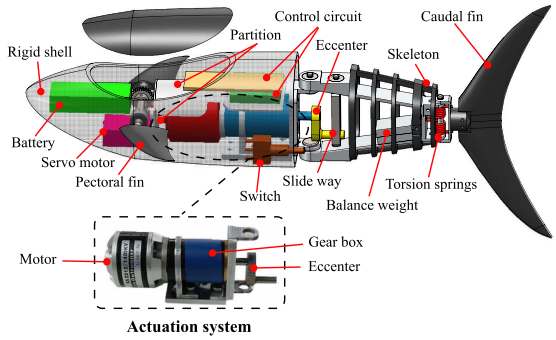

Fig. 1. Mechanical structure of the swimming robot.

Fig. 2. Prototype of the swimming robot.

II. Overview of the Swimming Robot

A. Overview of Mechanical Design

In the interest of achieving high-speed swimming motion and leaping motion, we develop a second-generation swimming robot with the integration of high-frequency oscillation and compliant mechanism. The miniaturization and lightweight design philosophies are employed. As illustrated in Fig. 1, the body profile of the robot is designed with a well-streamlined shape to reduce drags. A rigid head is used to hold the electronic modules, such as micro-controller board, actuators, sensors, and so on. Furthermore, we select a radio frequency module to realize the communication between host computer and the robot. A pair of pectoral fins with one degree of freedom (DOF) is actuated by a compact servo motor to realize the pitching motion. For realizing the high-frequency oscillation, a single active joint and a passive joint are adopted to actuate the self-propelled body. In this design, a high-efficiency actuating mechanism, namely, translating continuous rotation of the powerful motor in one direction into the fish-like swimming motion with lateral oscillations of posterior body is employed, which ensures the implement of high-frequency actuation efficiently. Two identical torsion springs as the compliant components are integrated into the passive joint for performance improvement. The design of robot has been miniaturized to achieve the fast-swimming motion and the leaping motion.

B. Fabrication of Prototype

The prototype of our swimming robot is shown in Fig. 2. An elastic skin made of emulsion is adopted as the waterproofing process. In order to support the elastic skin for a streamlined

TABLE I
TECHNICAL SPECIFICATIONS OF THE SWIMMING ROBOT

Items	Characteristics
Dimensions ($L \times W \times H$)	264 mm × 45 mm× 55 mm
Total mass	350 g
Actuators	Servo motor, Brushless motor
Communication mode	Wireless (RF, 433 MHz)
Control unit	STM32F405RG
No-load maximum frequency	18.5 Hz
Power supply	11.1V 180-mAh Li-ion battery

shape of posterior body, a 3D-printed skeleton is employed. In the position of joints, we left enough length of skin to reduce its drags in the oscillation, which ensures the less effects of elastic skin on providing additional stiffness. Based on the first-generation swimming robot, some improved designs are conducted to achieve better swimming performance. First, a powerful outrunner brushless direct current (BLDC) motor (EMAX, XA2212, 1400 KV, weight, 52 g) is selected as the actuator, which has a recorded output power of 247.2 W [24]. With the gear box (maxon GP 22 C, reduction gear ratio, 14:1, weight, 55 g), the calculable power density is 2.3 kW/kg which is superior to the motor used in previous robotic fish. Second, with some trials of different lengths of posterior body, the link with a length of 65 mm is selected, which allows the robot to become smaller in size and lighter in weight. In addition, a tuna-inspired caudal fin with a high aspect ratio of 8.05 is designed to connect the compliant passive joint. Finally, the designed robot is 264 mm in length and 350 g in weight. Thereinto, 25-gram balance weight is used for symmetrical mass distribution. The technical specifications are tabulated in Table I.

III. OPTIMIZATION EXPERIMENTS OF SWIMMING PERFORMANCE

With the developed second-generation swimming robot, in this section, extensive experiments were performed to analyze the effects of compliant components under a wide range of oscillation frequencies on swimming performance.

A. Design of Experiments

In the design of swimming robot, the high-frequency oscillation and compliant passive mechanism are two critical points for the high-speed swimming. The compliant joint with torsion springs can modulate the power transmitted to caudal fin to generate more peak thrust in return stroke [19]. The effect of power modulation is usually governed by the stiffness. In our design, it is determined by spring constants. To explore the effects of compliant components on swimming performances, different stiffness of compliant joint and caudal fin are employed to conduct experiments. Specifically, in order to simplify the experiments and ensure the improvement of swimming speed, we finally choose four cases, as presented in Table II. Three torsion springs with different stiffness are selected. Additionally, a soft caudal fin is constructed from Carbon Fiber Reinforced Composites (CFRP) with an estimated stiffness of 75 N/m. A rigid caudal fin is 3D-printed with a given chordwise cross section of NACA 0018 airfoil. The stiffness is estimated as 2635 N/m.

TABLE II
SPECIFICATIONS OF FOUR CASES OF COMPLIANT COMPONENTS

Case name	JN1-R	JN1-S	JN2-S	JN3-S
Stiffness of joint K_s (g·mm/°)	170	170	330	600
Caudal fin	Rigid	Soft	Soft	Soft

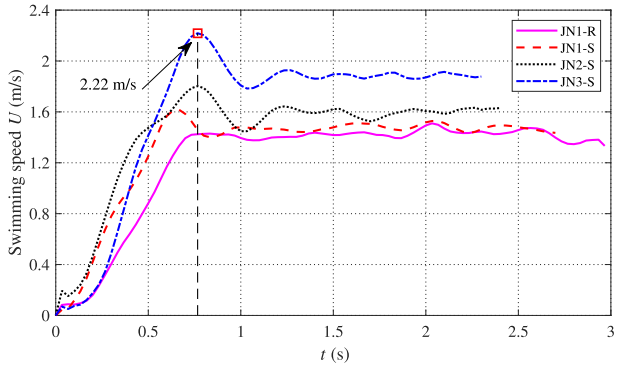

Fig. 3. Swimming speed curves of four cases at each maximum tail-beating frequency.

TABLE III
MAXIMUM STEADY SPEEDS OF THE SWIMMING ROBOT WITH FOUR CASES

Case name	JN1-R	JN1-S	JN2-S	JN3-S
Frequency (Hz)	15.25	15.09	14.39	15.04
Speed (SD, m/s)	1.43 (0.044)	1.48 (0.027)	1.60 (0.037)	1.88 (0.016)

B. Steady Speed of Free Swimming Motion

The free swimming speed is measured in water tank with a size of 5 m×4 m×1.2 m. In the experiments, the head of robot pastes red markers for detecting the position. A global vision camera (Daheng Imaging, MER-132-43U3C, 1292×964, 30 fps) is installed above the pool to record the planar motion of our robot in real time. A motion measurement system developed in our previous work [25] is adopted to analyze the swimming speed. The turning swimming motion is not considered in the mechanical design, therefore, the bilateral symmetry is necessary for the realization of relatively straight swimming. The robot keeps a little positive buoyancy for better stability in high-speed swimming, so the experiments were conducted on water surface.

In this study, the steady speed is utilized to evaluate the swimming speed, which is defined as the average swimming speed of the last two fifths time interval where the swimming speed has varied gently. The maximum swimming speed curves varying with time for four cases are shown in Fig. 3 and the detailed steady speeds with standard deviations (SD) are tabulated in Table III. JN3-S results in excellent maximum speed of 2.22 m/s (8.4 BL/s) and steady speed of 1.88 m/s (7.1 BL/s) at the frequency of 15.04 Hz, respectively. Fig. 4 shows the

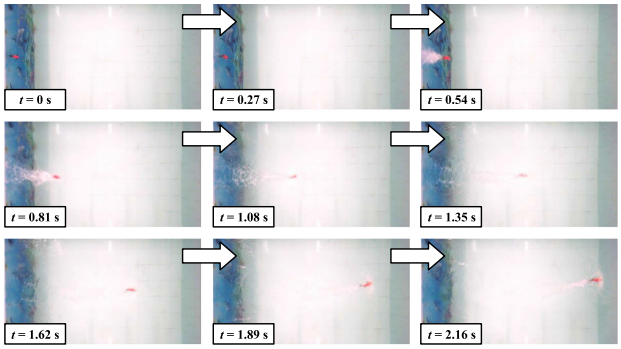

Fig. 4. Snapshot sequence of free swimming for the robot with JN3-S at a frequency of 15.04 Hz.

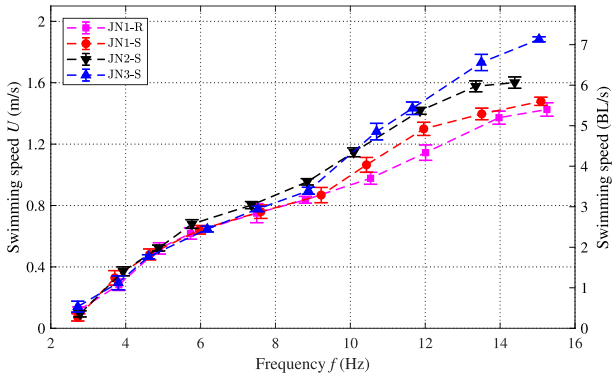

Fig. 5. Steady speed curves of four cases at different frequencies.

corresponding snapshot sequence of free swimming motion. The improvement of maximum speed is outstanding and about 0.45 m/s (1.7 BL/s).

The steady speeds of four cases at different oscillation frequencies are presented in Fig. 5. With the increase of tail-beating frequency, the steady speeds all increase remarkably. When the frequency is lower, the differences of swimming speeds for four cases are not obvious. However, as the frequency increases, the speeds emerge apparent differences. At lower frequencies, the deflection angles of passive joint are all small, which results in the insignificant influences of compliant joint. When the frequency is higher, the deflection angle trends to be large, and the influence of compliant joint becomes prominent in the speed improvement. That is to say, the optimization of stiffness is particularly significant in the improvement of speed at high frequency. The case of JN1-S obtains a little higher swimming speed than the case of JN1-R, therefore, we give up the cases of JN2-R and JN3-R with the rigid caudal fin. According to Fig. 5, it seems that the swimming speed of our robot will be improved by increasing the actuation frequency and stiffness of compliant joint until the optimal conditions are reached. However, the size of joint and the power of actuator limit the increase of torsion springs' stiffness and tail-beating frequency, respectively. The further optimization of our robot is not considered in this letter.

As a widely used indicator in biomimetics, swimming number *Sw* is used to evaluate the propulsion performance of our robot

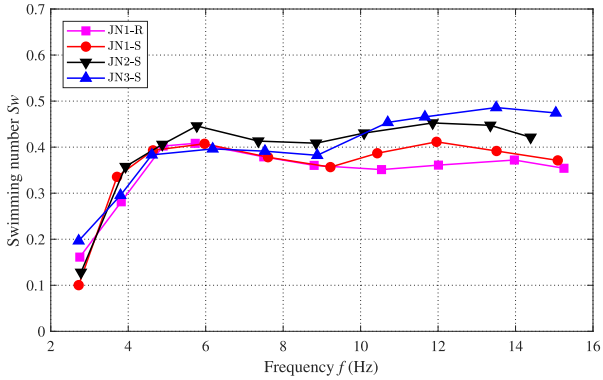

Fig. 6. Comparisons of swimming number *Sw* between the swimming robot with four cases at different tail-beating frequencies.

as below [26].

$$Sw = \frac{U}{fL} \tag{1}$$

where U is the swimming speed, f denotes tail-beating frequency, L represents the body length of robot.

Swimming number *Sw* indicates the relative distance travelled per tail beat. In general, it is about 0.6 for high performances [26]. The swimming number of our robot is shown in Fig. 6. The maximum *Sw* is about 0.49 and obtained with JN3-S. When frequency is greater than 10 Hz, the joint with larger stiffness results in higher swimming number and trends to close to the value of 0.6, which indicates that the stiffness optimization of compliant component has refined the propulsion performance of our robot.

C. Power Measurement

Energy consumption is a significant performance for the swimming robot. In the experiments, voltage and current signals of the battery were measured by a voltage sensor module and current module, respectively. A data acquisition (DAQ) device was used to record both signals synchronously with a rate of 1000 Hz. After dealing with signal data with moving average filter, the average power of four cases were calculated. It should be noted that owing to the constraint of space, we have to measure the power with a tethered situation, namely, the robot swims with two cables. The average power varying with frequency are illustrated in Fig. 7. With the increase of frequency, the power increases obviously, and JN1-R and JN1-S trend to consume the most power and least power, respectively. Due to the existing of cables, the maximum frequencies of four cases are all smaller than the maximum tail-beating frequencies in untethered cases. To calculate the COT at same frequency, we use the polynomial fitting method to describe the relationships between power and frequency (as presented in Fig. 7), as well as speed and frequency for each case, which causes lower efficiency than the untethered situation.

To evaluate the propulsive efficiency, the cost of transport (COT) denoting the consumed energy per unit distance travelled

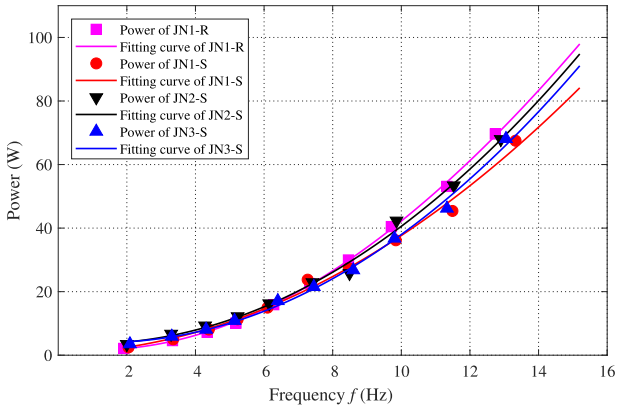

Fig. 7. Average power and fitting curves of the swimming robot with four cases.

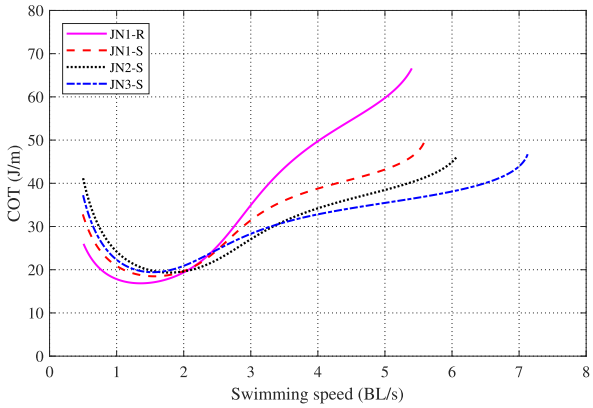

Fig. 8. COT versus swimming speed given in body length per second.

is calculated as follows:

$$\text{COT} = \frac{P}{U}, \tag{2}$$

where P denotes the power consumption.

As shown in Fig. 8, we present the relationship between COT and speed (BL/s) which ranges from 0.5 BL/s to the maximum speed of each case. The designed robot has U-shaped COT relationships with swimming speed, which is consistent with the work in [16]. It is interesting to note that at lower swimming speed, the robot with JN1-R is most efficient with minimum COT. When the swimming speed increases, the COT increases rapidly and the efficiency is lowest. JN1-R achieves the minimum COT of 16.86 J/m at the speed of 1.37 BL/s. With the carried 2-watt-hour battery, the robot can swim 427 m with duration time of 19.7 mins. As for JN3-S, the minimum COT is 19.43 J/m and obtained at 1.51 BL/s (370 m, 15.5 mins). When the speed exceeds about 3.4 BL/s, the COT of JN3-S trends much lower than other cases and the maximum COT is 45.81 J/m at 7.1 BL/s (157 m, 1.4 mins). From Fig. 8, we can find that the increase of stiffness contributes to the improvement of efficiency at high-speed swimming remarkably. Consequently, JN3-S obtains the maximum swimming speed and efficiency in high-frequency oscillation simultaneously.

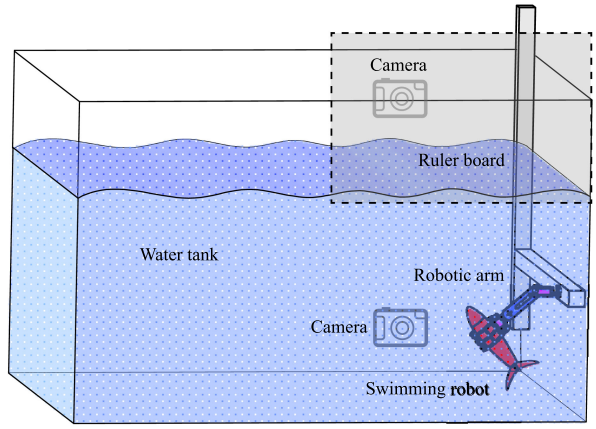

Fig. 9. Illustration of the measurement setup of leaping motion.

IV. Testing and Numerical Analysis of Leaping Motion

A. Performance Testing of Leaping Motion

During the leaping motion of fish, not only the caudal fin produces most thrust, but also the median fins and paired fins generate vertical acceleration, as well as posture stabilization [13]. However, in this letter, only a pair of pectoral fins with one DOF is designed, which makes it difficult to provide extra thrust and keep stable attitude in surfacing at high speed. Therefore, in order to focus on exploring the leaping performance, we built an experimental setup, as illustrated in Fig. 9. To simplify the measurement, a robotic arm including a gripper for holding the robot and a joint for adjusting the initial pitch angle is designed. One camera (FUJIFILM X-T20, 1920×1080, 60 fps) is fixed on the side of tank with appropriate position to capture the leaping motion in air. A GoPro (1920×1080, 120 fps) is also fasten to record the underwater swimming motion. A white board with a reference ruler is used as an auxiliary tool for displaying the leaping height intuitively.

Ultimately, the snapshot sequence of leaping motion in air is depicted in Fig. 10. In the experiments, we define the leaping height as the distance from water surface to the robot's CM. From Fig. 10, we can find that when $t = 167$ ms, the robot leaps out of water totally and the leaping height is about 0.10 m. When $t = 283$ ms, the robot achieves the maximum height of 0.23 m. Thus, the take-off speed U_t of robot at $t = 167$ ms can be estimated as

$$U_t = \sqrt{2g\Delta h} = 1.60\,\text{m/s}, \tag{3}$$

where $g = 9.81$ m/s^2 denotes the gravitational constant, $\Delta h = 0.13$ m indicates the difference in height.

In experiments, we analyze the underwater locomotion. At the beginning, the robot oscillates at high frequency with a given pitch angle and then is released by the gripper, which ensures it to accelerate towards water surface for performing the leaping motion. As shown in Fig. 11, we present the speed and depth curves which start from the beginning of oscillation to piercing water surface. At the time of 0.88 s, the robot was released to swim to water surface and the following acceleration motion is presented in Fig. 12. With the acceleration distance of 0.8 m, the

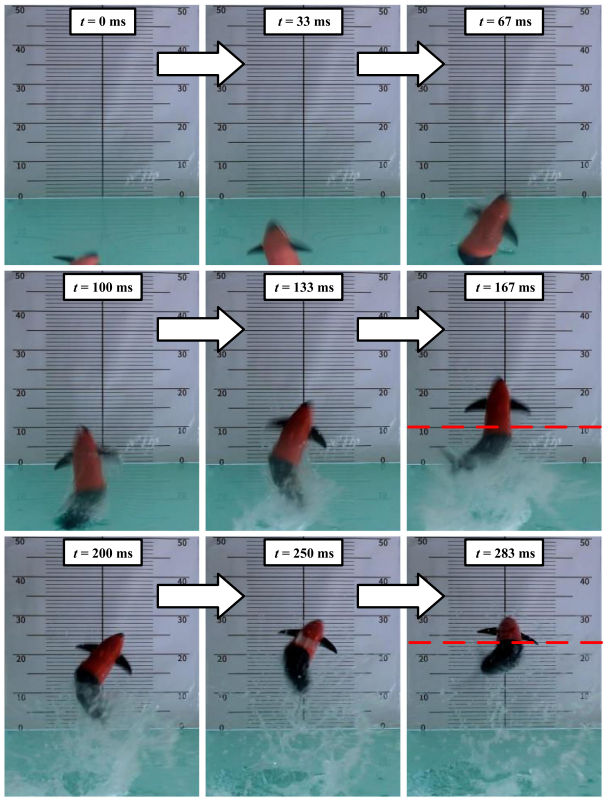

Fig. 10. Snapshot sequence of leaping motion for measuring the height.

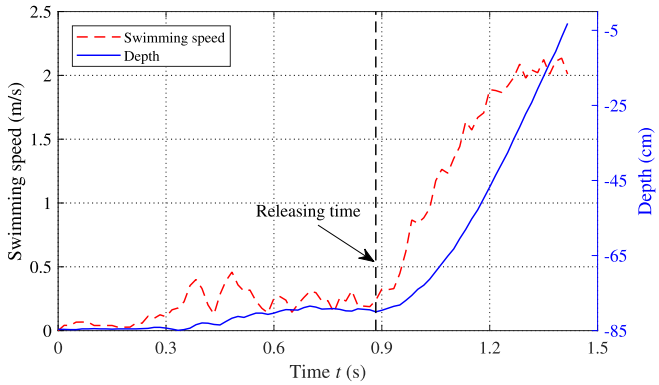

Fig. 11. Speed and depth curves of underwater acceleration motion.

robot reaches an exiting speed about 2.14 m/s. It should be noted that at the beginning, owing to the water pressure, the robot with a compressible rubber posterior body is negative buoyancy, only nearing water surface, the robot starts to become a little positive buoyancy. Thus, the buoyancy does not bring too much extra acceleration for leaping motion.

In the phase of crossing water surface, some water adheres to the robot, which adds the mass of robot. Especially, during the posterior body passes through water surface, large quantities of water splashes, which causes a clear drop of leaping speed and the unstable posture in air. Therefore, by coating super hydrophobic materials and optimizing the locomotion of crossing water surface, the leaping performance will be further improved.

B. Numerical Analysis of Leaping Performance

To analyze the leaping performance with swimming speed, a simplified numerical model is established. For the extreme complexity of leaping motion with fish-like oscillation, only vertical leaping motion is analyzed and the rotation is not considered. In the dynamic modeling, we define the leaping height l as the length from the top point of robot to water surface. In the leaping motion, there are mainly five forces exerting on the body: thrust (T), gravity (G), buoyancy force (B), drag force (F_d), and additional force from entrained fluid (F_f). For a fish-like swimming robot, the thrust is mainly generated by the oscillation of caudal fin. Therefore, we assume that before the caudal fin starting to emerge from water, the thrust remains constant, and then the thrust begins to decrease linearly to zero until it leaps out of water completely. In additional, we suppose the robot has achieved steady swimming before reaching water surface, which can be used to estimate the initial thrust.

The buoyancy force acting on the submerged body can be calculated as $B = \rho g V_{sub}$, where ρ is the density of water, V_{sub} indicates the volume of submerged body. The drag force acting on the submerged body is expressed as $F_d = 1/2\rho C_d A_{sub} {U_b}^2$, where C_d is the drag coefficient, A_{sub} represents the projected area of submerged body, $U_b = \dot{l}$ denotes the speed of body. It should be noted that the volume V_{sub} and area A_{sub} vary with the change of leaping height l. For the irregular shape of robot, we utilize SolidWorks to measure the volumes and areas of submerged body at different leaping heights and obtain the functions $V_{sub}(l)$ and $A_{sub}(l)$ with the fitting method, as shown in Fig. 13.

In the water-exit process, the robot still oscillates to produce thrust, for which large quantities of spray are splashed. We simplify it as the force generated by added fluid (additional water carried by emerged body) as $F_f = m_f(l)g + m_f(l)\ddot{l}$. Therefore, we also model the mass $m_f(l)$ as the added mass in the following form:

$$m_f(l) = \int_0^l \frac{1}{4} c_m \rho \pi h(l)^2 dl, \tag{4}$$

where c_m is the dimensionless coefficient, $h(l)$ represents the width of body at the interface between water and air.

Finally, before leaping out of water completely, the equation of leaping motion can be expressed as

$$(m_b + m_a)a = T + B - G - F_d - F_f, \tag{5}$$

where m_b is the mass of robot, m_a is the added mass acting on the submerged body, $a = \ddot{l}$ is the acceleration of body.

With the measured initial speed of 2.14 m/s, we estimate the leaping performance with the numerical model. The calculated take-off speed U_{ts} is about 1.8 m/s and the height of CM is about 0.31 m, which are larger than the experiment results. We attribute it to the simplification of dynamic model in many aspects, especially, the drags in generating spray are more obvious. Additionally, the robot also does not perform a completely vertical leaping and there are also some measurement errors in the experiments.

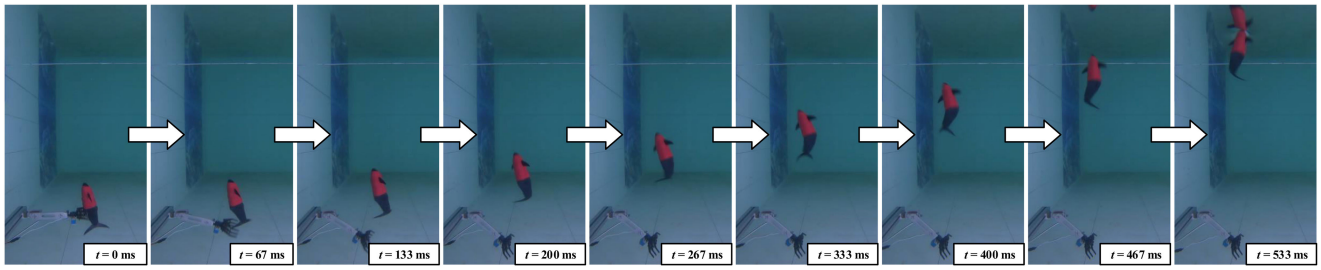

Fig. 12. Snapshot sequence of underwater acceleration motion.

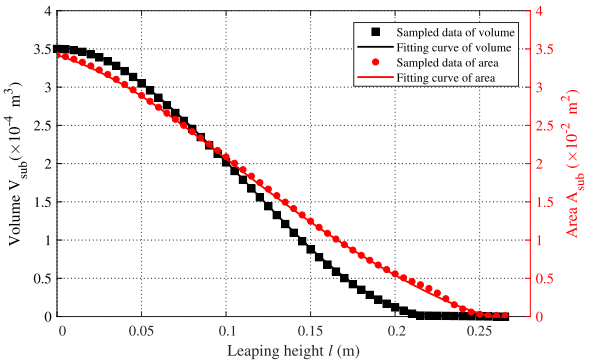

Fig. 13. Volume and area of emerged body against the leaping height l.

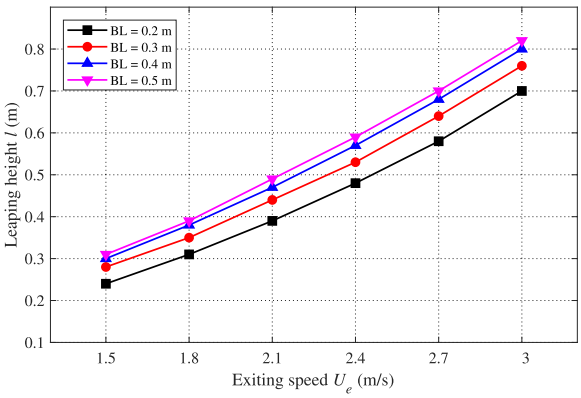

Fig. 14. Numerical estimation of leaping height l of four robots with different exiting speeds.

Based on the numerical model, we analyze the leaping performance of four robots with the body length of 0.2 m, 0.3 m, 0.4 m, and 0.5 m, respectively. Assume that these robots have the same volume and area distributions. By the normalization processing of the obtained volume and area functions, we can also get the volume and area functions of four robots, respectively. The estimated leaping height at different exiting speeds is presented in Fig. 14. The height increases with the exiting speed. At the same exiting speed, the larger robot achieves a higher leaping height l, which is due to a larger thrust is obtained and the duration time of propulsion is longer. However, a smaller robot is easier to leap out of water completely ($l \geq$ BL). The lightweight robot is more suitable for the compatible design of an aquatic-aerial robot, which also needs to possess the capability of locomotion in air. Note that the dynamic model is only intended to analyze some variation tendencies of leaping performance with the speed and body length, which will be useful to guide the design of robot with the capability of cross-domain motion.

V. Discussion

In this letter, we have developed an untethered swimming robot for high performance. By optimizing the stiffness of compliant components, the robot achieves remarkable free swimming speed. The comparisons of performance are summarized in Table IV, in which the most typical swimming robots with high speed are selected. As for the performance in speed, only iSplash-II exceeds our robot. However, with the miniature design in weight and length, our robot can leap out of water completely, which extends its application prospect considerably. It is worth noting that the robotic dolphin can also achieve leaping motion, but there are some different characteristics. Owing to the limited swimming speed, the robotic dolphin realizes leaping motion with precise posture control. However, our robot depends only on the impressive swimming speed to perform the leaping motion. We have improved the design of first-generation robot and optimized the stiffness of compliant joint experimentally. Relating to our previous robot [19], the robot in this work achieves a speed of 7.1 BL/s (1.88 m/s), increasing 3.3 BL/s (about 87%), a leaping height of 0.23 m (improving 0.09 m, 64%), and a maximum swimming distance of 427 m (increasing 86 m, 25%). In this letter, the efficiency has been improved significantly with the stiffness optimization, especially in high frequency oscillation. However, the power consumption is still larger than Tunabot and Tunabot Flex. There are many reasons accounting for this phenomenon, such as the spray generated by caudal fin, the serious mechanical wear of transmission shaft, and the tethered power measurement. A tunable stiffness joint was designed to realize the improvement of efficiency in [23]. In this study, we mainly focus on the improvement of speed with the stiffness optimization. Even its efficiency is also higher than our robot, the locomotion capabilities of our robot, such as speed and leaping performance, are much better.

Compared with the previously reported water surface jumping robots, our robot has obvious advantages in free swimming speed, leaping height, and large scale, which provides a great potential to carry sensors to execute tasks in complex aquatic environment. In addition, the small size and light weight allow our robot to evolve into an aquatic-aerial robot, such as flying

TABLE IV
PERFORMANCE COMPARISONS WITH THE EXISTING SWIMMING ROBOTS

Swimming robot	Mass (kg)	Length (m)	Frequency (Hz)	Speed (BL/s)	Swimming freely	Leaping motion
iSplash-II [15]	0.835	0.32	20.0	11.6	Yes	No
Tunabot [16]	0.306	0.255	15.0	4.0	No	No
Tunabot Flex [17]	0.19	0.255	8.0	4.6	No	No
Robotic dolphin [18]	4.7	0.72	4.65	2.85	Yes	Yes
Our previous robot [19]	0.38	0.277	12.82	3.8	Yes	Yes
Our robot in this study	0.35	0.264	15.04	7.1	Yes	Yes

fish. In brief, the overall performance of our robot is outstanding among these robots.

VI. CONCLUSION AND FUTURE WORK

In this letter, we have developed an untethered swimming robot with the capability of high-speed swimming and fish-like leaping. By integrating the high-frequency actuation system and compliant passive mechanism, the prototype is fabricated with a compact size of 264 mm in length and 350 g in weight. The effects of compliant components' stiffness on swimming performance are analyzed by extensive experiments. The results indicate that by optimizing the stiffness, both swimming speed and efficiency are significantly improved and a maximum swimming speed of 7.1 BL/s is achieved. Finally, the fish-like leaping is successfully performed and the locomotion is analyzed. The maximum leaping height of CM is about 0.23 m. Compared with the existing swimming robots and water surface jumping robots, our robot has demonstrated its superiority. A simple numerical analysis is also conducted to reflect the influence of speed and body length on leaping performance. This research will contribute to the innovative design of high-performance swimming robots and water leaping robots. In our future work, we will mainly focus on the design of foldable pectoral fins to develop a robotic flying fish for the realization of gliding motions in air.

REFERENCES

[1] D. T. Roper, S. Sharma, R. Sutton, and P. Culverhouse, "A review of developments towards biologically inspired propulsion systems for autonomous underwater vehicles," *Proc. Inst. Mech. Eng. M: J. Eng. Marit. Environ.*, vol. 225, no. 2, pp. 77–96, May 2011.

[2] J. Yu, L. Wen, and Z. Ren, "A survey on fabrication, control, and hydrodynamic function of biomimetic robotic fish," *Sci. China Technol. Sci.*, vol. 60, no. 9, pp. 1365–1380, Jun. 2017.

[3] A. Raj and A. Thaku, "Fish-inspired robots: Design, sensing, actuation, and autonomy-A review of research," *Bioinspir. Biomim.*, vol. 11, no. 3, Apr. 2016, Art. no. 031001.

[4] F. Berlinger, M. Gauci, and R. Nagpal, "Implicit coordination for 3D underwater collective behaviors in a fish-inspired robot swarm," *Sci. Robot.*, vol. 6, no. 50, Jan. 2021, Art. no. eabd8668.

[5] G. Li *et al.*, "Self-powered soft robot in the Mariana Trench," *Nature*, vol. 591, no. 7848, pp. 66–71, Mar. 2021.

[6] A. Vidyasagar, J. C. Zufferey, D. Floreano, and M. Kovač, "Performance analysis of jump-gliding locomotion for miniature robotics," *Bioinspir. Biomim.*, vol. 10, no. 2, Mar. 2015, Art. no. 025006.

[7] J. K. Yim, B. R. P. Singh, E. K. Wang, R. Featherstone, and R. S. Fearing, "Precision robotic leaping and landing using stance-phase balance," *IEEE Robot. Autom. Lett.*, vol. 5, no. 2, pp. 3422–3429, Apr. 2020.

[8] J. Yan, K. Yang, T. Wang, X. Zhang, and J. Zhao, "A continuous jumping robot on water mimicking water striders," in *Proc. IEEE Int. Conf. Robot. Autom.*, Stockholm, Sweden, 2016, pp. 4686–4691.

[9] F. Jiang, J. Zhao, A. K. Kota, N. Xi, M. W. Mutka, and L. Xiao, "A miniature water surface jumping robot," *IEEE Robot. Autom. Lett.*, vol. 2, no. 3, pp. 1272–1279, Jul. 2017.

[10] Y. Chen *et al.*, "A biologically inspired, flapping-wing, hybrid aerial-aquatic microrobot," *Sci. Robot.*, vol. 2, no. 11, Oct. 2017, Art. no. eaao5619.

[11] R. Zufferey *et al.*, "Consecutive aquatic jump-gliding with water-reactive fuel," *Sci. Robot.*, vol. 4, no. 34, Sep. 2019, Art. no. eaax7330.

[12] B. Chang, J. Myeong, E. Virot, C. Clanet, H. Y. Kim, and S. Jung, "Jumping dynamics of aquatic animals," *J. R. Soc. Interface*, vol. 16, no. 152, Mar. 2019, Art. no. 20190014.

[13] A. M. Shih, L. Mendelson, and A. H. Techet, "Archer fish jumping prey capture: Kinematics and hydrodynamics," *J. Exp. Biol.*, vol. 220, pp. 1411–1422, Apr. 2017.

[14] J. Davenport, "Wing-loading, stability and morphometric relationships in flying fish (Exocoetidae) from the north-eastern atlantic," *J. Mar. Biolog. Assoc. U.K.*, vol. 72, no. 1, pp. 25–39, Feb. 1992.

[15] R. J. Clapham and H. Hu, "*iSplash*: Realizing fast Carangiform swimming to outperform a real fish," in *Proc. IEEE/RSJ Int. Conf. Intell. Robot. Syst.*, Chicago, USA, 2014, pp. 1080–1086.

[16] J. Zhu, C. H. White, D. K. Wainwright, V. Di Santo, G. V. Lauder, and H. Bart-Smith, "Tuna robotics: A high-frequency experimental platform exploring the performance space of swimming fishes," *Sci. Robot.*, vol. 4, no. 34, Sep. 2019, Art. no. eaax4615.

[17] C. H. White, G. V. Lauder, and H. Bart-Smith, "Tunabot flex: A tuna-inspired robot with body flexibility improves high-performance swimming," *Bioinspir. Biomim.*, vol. 16, no. 2, Mar. 2021, Art. no. 026019.

[18] J. Yu, Z. Su, Z. Wu, and M. Tan, "Development of a fast-swimming dolphin robot capable of leaping," *IEEE/ASME Trans. Mechatronics*, vol. 21, no. 5, pp. 2307–2316, Oct. 2016.

[19] D. Chen, Z. Wu, Y. Meng, M. Tan, and J. Yu, "Development of a high-speed swimming robot with the capability of fish-like leaping," *IEEE/ASME Trans. Mechatronics*, to be published, doi: 10.1109/TMECH.2021.3136342.

[20] M. Ziegler, M. Hoffmann, J. P. Carbajal, and R. Pfeifer, "Varying body stiffness for aquatic locomotion," in *Proc. IEEE Int. Conf. Robot. Autom.*, Shanghai, China, May 2011, pp. 2705–2712.

[21] B. Chen and H. Jiang, "Body stiffness variation of a tensegrity robotic fish using antagonistic stiffness in a kinematically singular configuration," *IEEE Trans. Robot.*, vol. 37, no. 5, pp. 1712–1727, Oct. 2021.

[22] K. Li, H. Jiang, S. Wang, and J. Yu, "A soft robotic fish with variable-stiffness decoupled mechanisms," *J. Bionic Eng.*, vol. 15, no. 4, pp. 599–609, Jul. 2018.

[23] Q. Zhong *et al.*, "Tunable stiffness enables fast and efficient swimming in fish-like robots," *Sci. Robot.*, vol. 6, no. 57, Aug. 2021, Art. no. eabe4088.

[24] YINYAN Model Tech MFT. LTD., "XA2212 Brushless Motor+Accessories (yinyanmodel.com)," Accessed: Aug. 25, 2021. [Online]. Available: http://www.yinyanmodel.com/En/ProductView.asp?ID=270

[25] J. Yuan, J. Yu, Z. Wu, and M. Tan, "Precise planar motion measurement of a swimming multi-joint robotic fish," *Sci. China Inf. Sci.*, vol. 59, no. 9, Sep. 2016, Art. no. 92208.

[26] W. Zhao, A. Ming, and M. Shimojo, "Development of high-performance soft robotic fish by numerical coupling analysis," *Appl. Bionics Biomech.*, vol. 2018, Nov. 2018, Art. no. 5697408.